6.1 Introduction

Glucose is an essential component for human beings because it makes available energy for cell metabolism and maintains the regular operation of biological function. The excess glucose level in the body lead to diabetes [Zhang et al., 2023; El Safty et al., 2020]. The International Diabetes Federation (IDF) estimates that more than 400 million individuals worldwide have diabetes [Cho et al., 2018]. Diabetes is a disease that cannot control the blood glucose level in people's bodies. According to the World Health Organization, the normal fasting blood glucose range is 4-6 mM, and in urine, the normal glucose range is 0-0.8 mM [Pandey et al., 2021]. For people with diabetes, chronic damage and dysfunction of their tissues, particularly of their eyes, kidneys, hearts, blood vessels, and nerves, are easily caused by long-term hyperglycemia. The current pandemic of COVID-19 has significantly affected glucose in patients with diabetes [Nassar et al., 2021]. Diabetic patients were at higher risk for COVID infection due to weak immune systems [Abi et al., 2020; Lim et al., 2021]. What's worse, the condition can lead to other issues, including blindness and kidney failure, all brought on by an excess of glucose in the human blood [Zhu et al., 2021]. Thatswhy, the early detection and effective treatment of diabetes are of great significance for developing a technique for the analytical determination of glucose content. Several prominent publications have been reported on glucose detection, and research is still going on based on various technologies and devices, such as electrochemical [Gijare et al., 2021], colorimetric [Nirala et al., 2018], fluorometric [Shen et al., 2014], and chemiluminescence [Yang et al., 2021] methods. Most of these methods find good sensitivity with glucose, but still, these methods have some demerits, such as tedious operation, slow response speed, and severe analysis conditions. The chemiluminescence technique has attracted much attention due to its simplicity, high sensitivity, accuracy, and ease

of operation [Huang et al., 2022]. However, contemporary analytical techniques have several flaws, including low sensitivity, sophisticated instrumentation, and time taking processes [Reda et al., 2021; Zhu et al., 2016]. That's why developing an easy-to-use, sensitive technology for measuring blood glucose is crucial. We generally need blood serum for its detection, which is painful. So non-invasive techniques may be a breakthrough in the sensing field. Also, this non-invasive glucose monitoring methodology can overcome the shortcomings of the present invasive, costly, painful, and burdensome glucose monitoring systems. Conventional enzymatic-based sensors can measure glucose concentration, but they have a limitation due to the poor stability and activity of enzymes [Bi et al., 2023]. Enzyme glucose oxidase (GOx) is utilized for the sensing of glucose, but it finds a demerit due to poor activity below pH two and above pH eight, and also temperatures above 40 $^\circ$C have no good response [Gao et al., 2021]. Things need to be updated, and now we are analyzing glucose non-invasively and non-enzymatically.

Herein, a visually attractive chemiluminescence-based sensor is created for the one-step, quick detection of glucose in human urine. Chemiluminescence (CL) is a type of luminescence phenomenon in which the emission of light is caused by a chemical reaction (exothermic), which results in an electronically excited intermediate gets decays to the ground state. A chemiluminescence signal has a shorter lifetime and shows low-emission radiation. Still, their stability has been effectively improved after introducing catalyst (e.g., metal or semiconductor nanoparticles, catalytic ions, enzymes) into the luminol system [Qi et al., 2013]. The catalyst may be CeO_2 nanoparticles [Huang et al., 2021], ZnO nanoparticles [Li et al., 2009], or CuO nanoparticles [Chen et al., 2012]. In other cases, researchers have done noticeable works around catalyzed CL systems by using noble metal nanoparticles, such as Au, Pt, and Ag

nanoparticles, that improve the inherent sensitivity performance and selectivity of traditional CL systems [Wang et al., 2020]. Among catalytically active metal nanomaterials, gold nanoparticles were broadly utilized in biosensing programs, due to which it has exciting optoelectronic property satisfactory tuning through minor adjustments within the shape, size, morphology, and surface capability [Zhang et al., 2005; Aslan et al., 2009]. Along with these properties, gold nanoparticles are biocompatible, non-toxic, and have good biological affinity [Liu et al., 2016].

To the paramount of our understanding, a chemiluminescence imaging system has not yet been implemented for non-invasive glucose sensing based on a smartphone detection assay. Chemiluminescence is one of the significant tools to develop the diagnostic operation in complex media through the amplified eCL signals, used to intensify the sensitivity in assessment to traditional colorimetric probes. The Chemiluminescence technique integrated with smartphones has been a breakthrough in the sensing field. It is feasible and cost-effective and does not involve any sophisticated instrumentations. Detection of glucose via smartphones plays a crucial role in the recreation of a new kind of portable sensor device in healthcare [Vashist et al., 2014]. Further, smartphones can be extended with additional accessories and built-in functions with cloud services that make it more useful to sense different biomolecules, considered point-of-care (POC) devices. They could perform the test on-site (outside laboratories), even at a minimum cost, with fewer serious and emergency medical attention resources [Salimi et al., 2021]. From the literature screening, scientists have investigated several approaches for detecting biomarkers and clinically important analytes in biological fluids (sweat, saliva, and blood) [Lee et al., 2014; Oncescu et al., 2013].

Plenty of work has been done using GNPs for enhanced CL (eCL), offering a range of new ultrasensitive biosensor systems [Gijare et al., 2021; Bui et al., 2018; Wang et al., 2018]. Nirala et al. [Yang et al., 2009] demonstrated different size-dependent gold nanoparticles with enhanced CL for ultra-Sensitive sensing-based enhanced luminol chemiluminescence (CL) system [Nirala et al., 2019]. Another author reported non-enzymatic glucose detection in complex media through electrochemiluminescence based on the quenching impact on luminol using attapulgite–TiO_2. There has been an intake of dissolved O_2, exhibiting a quenching impact that could materialize at the luminol eCL emission [Wang et al., 2016; Shahrajabian et al., 2016; Roda et al., 2014].

Herein, we report eCL imaging for the first time and quantify the glucose analyte in urine (biological/biotic fluid) using a readily available smartphone based on the oxidase mimetic behavior of GNPs-PDT. The developed smartphone eCL sensor revealed susceptible eCL imaging quenching responses for the detection of glucose and supportive mechanism illustrated in Scheme 1. The synthesized GNPs cross-linked with thiol linker PDT, which acts as oxidase mimetic activity on the luminol-O_2 system. While in spiked glucose urine, the oxidation of glucose takes place in the presence of GNPs-PDT and generates oxygen radicals ($O_2^{\bullet-}$), which were used up in order that we get a quench in the eCL imaging signal, analyzed with image J software. The quenching intensity of eCL imaging was dynamically associated with the glucose concentration, and a developed sensor for glucose sensing could be achieved. The GNPs-PDT, as engineered nanomaterial, acts as a sensitive and robust catalyst due to a stable and strong eCL signal.

6.2 Materials and methods

Sodium borohydride (NaBH$_4$), Sodium luminol chloride, HAuCl$_4$, NaOH, Trisodium citrate, Glucose, Fructose, Lactose, Mannose, Sodium chloride, Potassium chloride, Ammonium phosphate have been purchased from Sigma Aldrich. The Milli-Q water and analytical grade chemicals were used in all experiments. Human urine samples were collected from healthy volunteers and patients with their consent.

6.2.1 Methods

6.2.1.1 Synthesis of gold nanoparticle and GNPs-PDT

Following the procedure of Brown et al. [Brown et al., 1996], GNPs (size, 15 nm) were synthesized by reduction of gold salt (tetra chloroauric (III) acid (0.01% w/w)) in aqueous media where reductant is aqueous ice-cold sodium borohydride (250 µL) and 1% trisodium citrate (375 µL) solution as a capping agent in 25 ml of Milli Q water under vigorous shaking. The solution was saved and stirred up for 30 min at 25°C to achieve desired nanoparticles size. The synthesized GNPs are biocompatible and have unique optical properties [Liu et al., 2016]. Finally, the synthesized nanoparticles were cross-linked with 5 mM PDT (prepared in methanol solvent) for 5 min incubation. The cross-link of GNPs with PDT is time-dependent, so we used a freshly prepared cross-linked solution for each experiment [Nirala et al., 2019]. 1,3-Propane dithiol cross-linked gold nanoparticles are a type of nanoparticle that has been functionalized with PDT molecules to create a crosslinked network on the surface of the GNPs. This results in several unique properties that make them useful in a variety of applications. The main novelty of these crosslinked GNPs lies in their stability and reactivity. The designed

product GNPs-PDT shows improved biocompatibility by increasing aqueous solubility, good biological affinity, and enhanced CL signal intensity [Nirala et al., 2019].

6.2.1.2 Sensing of glucose in the human urine sample

The fresh urine sample was pretreated by centrifuging at 5000 rpm for 30 min, and the supernatant sample of urine was collected. Then the supernatant was diluted 5 times for further sensing of glucose. Different concentrations of glucose (0.25, 0.50, 0.75, 1, 1.5, 2 mM) were spiked in pretreated urine. 20 μL of this processed urine was pipetted into a 96-well black Elisa plate containing optimized luminol (250 μL) and GNPs-PDT (40 μL) solutions. Further, eCL imaging was performed using a smartphone camera by putting a plate inside the black box (Figure 6.8b). The captured images were analyzed by Image J software.

6.2.2 Instrumentations:

Absorption spectra were investigated by UV-Vis spectrophotometer (UV-2600, Shimadzu). The CL intensity level was attained with a SYNERGY/H1 Microplate reader (BioTek) by racking peak intensity. Transmission electron microscopy (TEM) FEI, TECHNAI G^2 20 TWIN (Czech Republic) was done for the investigation of structural morphology, elements distribution, and size at an accelerating voltage of 200 kV. eCL imaging was performed by using a black box and smartphone camera.

6.3 Results and discussion

6.3.1 GNPs Characterizations

Inset of Figure. 6.1a is showing the clear visible color changes of GNPs after modification with PDT. The color of GNPs is wine red while on crosslinking GNPs-PDT color becomes violet.

The crosslinking of the PDT molecule on the surface of the GNPs creates a stable and robust network that helps to prevent the particles from aggregating together. This stability makes them suitable for use in biological and medical applications, where the particles need to remain stable in the presence of biological fluids. The synthesized gold nanoparticles (GNPs) of controlled morphology are widely used in bio-sensing applications. Because it has unique optical (surface plasmonic resonance, SPR), catalytic properties, and easy surface modification, leading to changes in optical properties that can easily visualize by the naked eye [Nayak et al., 2018; Zeng et al., 2012]. We synthesized GNPs through reduction methods by sodium borohydride and sodium citrate. We treated synthesized colloidal GNPs with PDT in a controlled manner for cross-linking to enhance the catalytic efficiency of bare GNPs. Figure. 6.1a shows UV–Vis extinction spectra of colloidal spherical GNPs and modified GNPs, revealing a characteristic of SPR change. The spectra reveal a significant absorbance peak at 521 nm before treated GNPs, and after treatment with cross-linker as PDT (1,3-Propanedithiol), broadband with red-shift of longitudinal surface Plasmon peak at range of 525-580 nm obtained due to its excessive linking toward thiol groups on the outside of nanoparticles surfaces [Nirala et al., 2019; Kim et al., 2019]. Furthermore, to investigate the structural morphology of GNPs, Figure. (1 b, c) shows TEM images of GNPs and cross-linked GNPs-PDT. The sample for TEM analysis was prepared via drop casting material on a carbon TEM grid under a lamp for 4 hours and then kept in a desiccator overnight. TEM characterization can reveal the size, shape, and distribution of the crosslinked particles, as well as any changes in their surface chemistry.
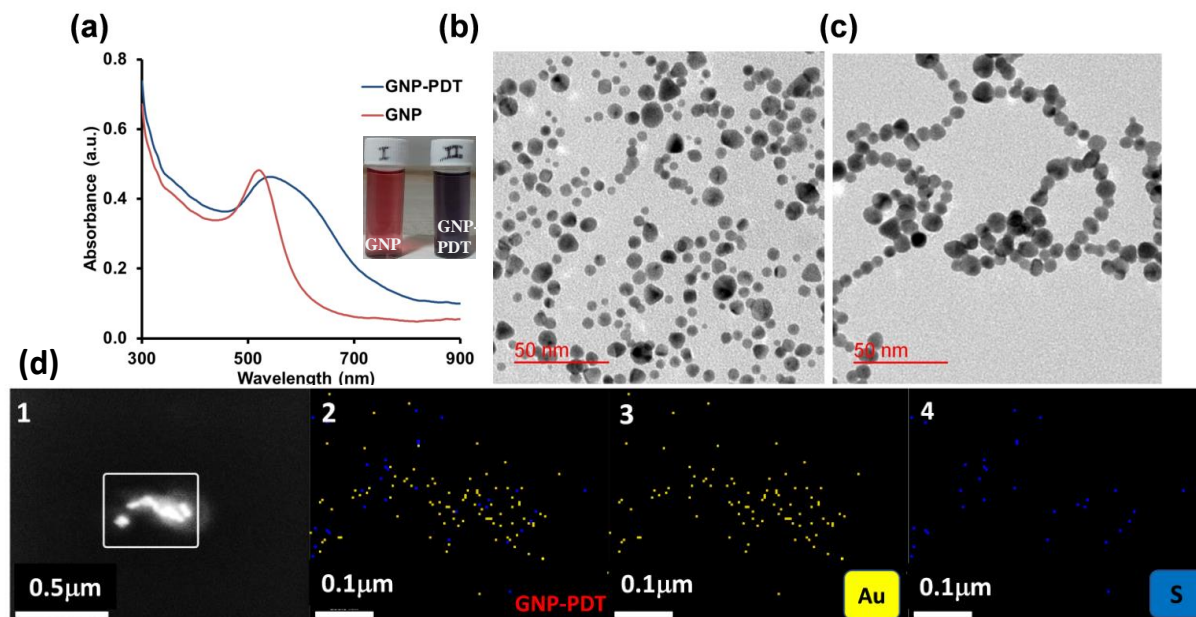
Figure 6.1 (a) UV-Visible spectra, (b) TEM image of GNPs, and (c) GNPs-PDT, (d) EDS mapping of composition of GNPs-PDT (where EDS = Energy-dispersive X-ray spectroscopy) (concentration = 268 μM, pH = 6)

Figure 6.1b and 6.1c state that we obtained highly dispersed and homogeneously spherical gold nanoparticles around 15 nm in size, and after treatment of colloidal GNPs with a cross-linker, PDT, which is disulfide moiety-induced self-assembled complex as GNPs-PDT into the form of the chain [Fernandes et al., 2010]. The chain-like network may be the formation of GNPs-PDT due to strong interaction between Au-S due to high gold and sulfur binding efficiency [Xi et al., 2015], which was certified with longitudinal SPR band observed in the self-assembly GNPs. The bandgap of GNPs and GNPs-PDT was calculated as (1.92 eV) and (1.62 eV), respectively, through the Tauc plot (Figure 6.2). The decrement in bandgap showed the shift of Fermi level towards the conduction band and increment in catalytic property of GNPs-PDT [Jupally et al., 2011; Subramanya et al., 2000]. Further elemental analysis has been done by using EDS mapping which shows homogeneously distributed gold and sulfur in the GNPs-

PDT. Figure. 6.1(d-1) depicts the STEM image corresponding to which the elemental mapping has been performed. Figure 6.1(d-2) represents the elemental distribution in the synthesized material. Figure 6.1 (d3&4) shows the distribution of Au and S (designating PDT) in the materials respectively. In our case, 5 min was sufficient for cross-linking of GNPs, potentially enhancing the eCL imaging signal within the luminol-O_2 system [Wang et al., 2020]. The cross-linked GNPs increase the stability of CL signal intensity as shown in Figure. 4a. In addition to their stability, the cross-linked GNPs exhibit enhanced reactivity compared to non-cross-linked GNPs. 1,3-propane dithiol molecules on the surface of the particles may act as thiol functional groups, which can bind to other molecules or surfaces.
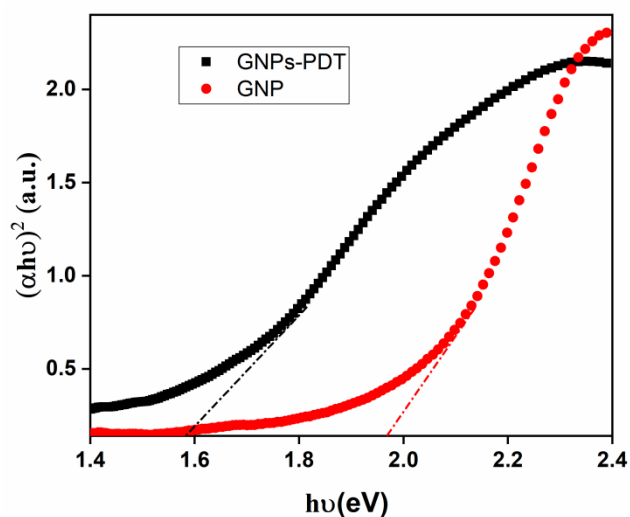

Figure 6.2 Tauc plot of GNP and GNPs-PDT.

6.3.2 Optimizations for eCL imaging

The optimum conditions for maximizing the CL emission intensity were determined for both luminol reagent and fabricated GNPs-PDT material. To obtain the optimized condition, the eCL imaging was recorded using a smartphone camera. Figure 6.3a shows the optimization of GNPs-PDT for eCL imaging by taking a series of volume of GNPs-PDT ((10µL, 20µL, 40µL,

60µL, 80µL, 100µL) keeping luminol (10 mg mL^{-1}) reagent fixed. further, we have optimized

the luminol concentrations (2, 6, 10, 12, 14 mg mL^{-1}) for achieving intense eCL imaging by

taking the fixed volume of the GNPs-PDT on Luminol-O$_2$ system. Hence, we are getting the

optimized volume as 30 µL for GNPs-PDT and the optimized concentration as 12 mg mL^{-1} for

luminol reagent (Figure 6.3b). The image was captured by a smartphone camera having ISO-

3200, acquisition time 30 sec, using a black box in the dark room. the captured image was

analyzed through Image J for quantification.
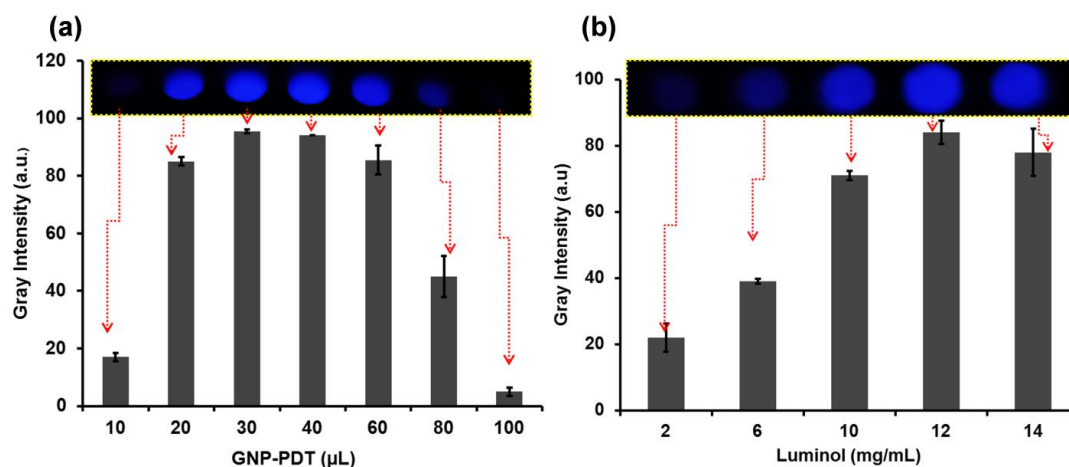
Figure 6.3 Optimization of eCL imaging on the luminol-O$_2$ system with (a) different volumes
of GNPs-PDT (b) Luminol (Room temperature)

Further, we have conducted several identical experiments using fresh solutions over different

days in order to test the reproducibility and stability of our proposed method. Figure 6.4 shows

the variation in sensor response over a week. From the result, it can clearly be inferenced that

sensor's activity is similar over one week without any significant variation in signal.
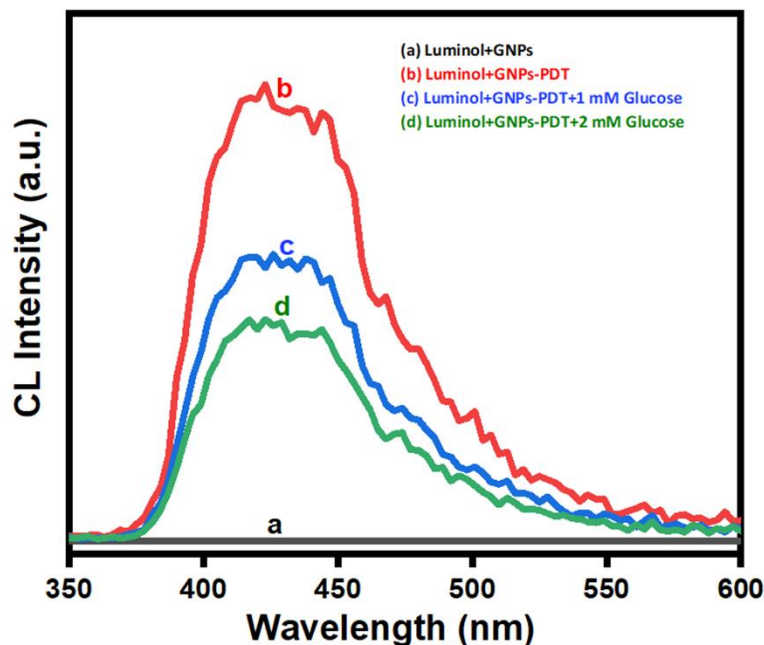
Figure 6.4 Chemiluminescence spectra of (a) Luminol + GNPs (b) Luminol + GNPs + PDT (c) Luminol + GNPs + PDT + 1 mM Glucose (d) Luminol + GNPs + PDT + 2 mM Glucose.

The metal nanoparticle's surface charge properties are crucial for the mechanism of luminol reaction to adorn catalytic interest for eCL imaging [Fan et al., 2012]. The citrate-decorated GNPs (conventional strategies) were used for eCL imaging; however, there is one drawback associated with weak eCL signal due to having a negative charge that electrostatically repels both oxide ions and anionic luminol [Zhang et al., 2005]. However, a less negative charge GNPs was synthesized by combining borohydride–citrate reduction [Nirala et al., 2019]. Moreover, the treatment of GNPs with cross-linking through PDT is attributed to a decrease in the total surface negative charge density related to non-cross-linked GNPs, as a result helping greater adsorption of anionic luminol on cross-linked GNP's surface [Oraby et al., 2017].

To evidence this assumption, we have demonstrated the possible molecular mechanism of the luminol-O_2 CL system in the presence and absence of catalyst. In the luminol-oxidant system, typically, five-amino-2, three-dihydropthalazine-1,4-dione as luminol molecules oxidized beneath fundamental situations by various oxidants or in the presence of oxygen to process an electronically excited-state three-aminophthalate anion (3-APA*), and it produces blue radiation (425 nm) whilst it deactivates to the electronic ground state. A broader look at the schematic in Figure 6.5 illustrates the possible mechanism involved in the catalysis of the luminol-O_2 CL system through PDT cross-linked GNPs.
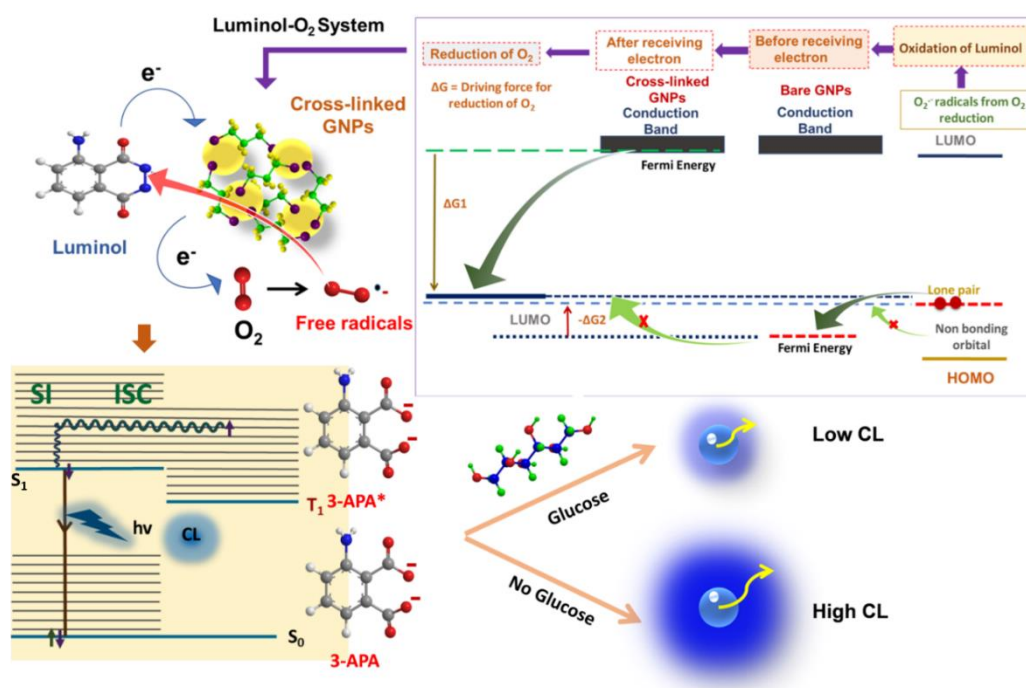

Figure 6.5 Schematic illustration of catalytic and sensing mechanism based on GNPs-PDT modified luminol-O_2 system. PDT treated GNPs accelerated reduction of O_2 for the formation of O_2 radicals, which leads to the oxidation of luminol and visualizing eCL signal by naked eyes in terms of CL imaging. In the presence of glucose, the inhibition effect of eCL imaging.

A transfer of electrons from the non-bonding orbital (NBO) of luminol dianion (L^{2-}) must be received with and without cross-linked GNPs, which have enough fermi energy to facilitate the transfer of electrons to the LUMO of O_2 for its reduction to superoxide radical anion. Without catalysis, eCL imaging or signal on luminol-O_2 was not observed due to a very weak signal [Borrego-Sánchez et al., 2020].

However, the mechanism demonstrated to facilitate electron transfers from the HOMO (NBO) of luminol double deprotonated dianion to the without cross-linked GNPs is not sufficient for thermodynamical reduction of dissolved molecular oxygen to superoxide radical anion [Giussani et al., 2019]. There could be a possibility of lower fermi energy without cross-linked GNPs, as shown in Figure 6.5. Due to cross-linking of GNPs with PDT, effective change in the valence and conduction band as well as shifting of Fermi energy levels towards the conduction band leading to facilitate the electron transfer from luminol dianion to the LUMO of molecular oxygen to generate superoxide radical anion ($O_2^{-\cdot}$), which combine with luminol to enhanced CL signal in term of imaging [Giussani et al., 2019; Yang et al., 2021]. Finally, the generated superoxide radical's anion ($O_2^{-\cdot}$) tends to attack the anti-bonding orbital (π^*) of the carbonyl group of luminol dianion (L^{2-}), resulting in the energetically high intermediate, hydroxy hydroperoxide (LOO⁻, Chemiluminophore) and N_2 molecules [Yang et al., 2021], and resulting active species 3-APA* (3-aminophthalate anion) has energy corresponding to triplet state (T_1) undergoes two radiation less processes, one is intersystem crossing (ISC), and other is a spin inversion (SI) and comes to the first excited singlet state (S_1) and then spontaneously deactivates to the electronically ground singlet state (S_0), 3-APA with the illumination of the blue radiation corresponding to wavelength 425nm [Barni et al., 2007]. Further, the above system has been applied for sensing glucose based on the inhibition of luminol CL intensity.

There are two steps involved in the eCL imaging of glucose in a biological fluid. One is the reduction of molecular oxygen, and the other is the oxidation of luminol catalyzed by cross-linked GNPs, resulting in enhanced CL reactions. The eCL signal was ceased as shown in the case of glucose addition indicating the necessity and presence of superoxide anion or oxygen-free radical O_2^- for completing the CL catalytic reaction. It may be quite possible that the utilization of active oxygen species for the oxidation of glucose causes the quenching of the CL signal [Wang et al., 2022].

6.3.3 eCL imaging of glucose on a Smartphone PRO camera in a biological fluid (urine)

A developed, optimized eCL imaging platform was used for imaging Glucose in the real sample based on the enhanced CL signal inhibition in the presence of glucose. The enhanced CL may be visualized by snapping images using a smartphone PRO camera and quantified by Image J analysis. First, we have done proof of concept for eCL imaging under optimized conditions; Figure. 6.8a reveals stability and enhanced eCL imaging signal [Liu et al., 2017; Shen et al., 2020].
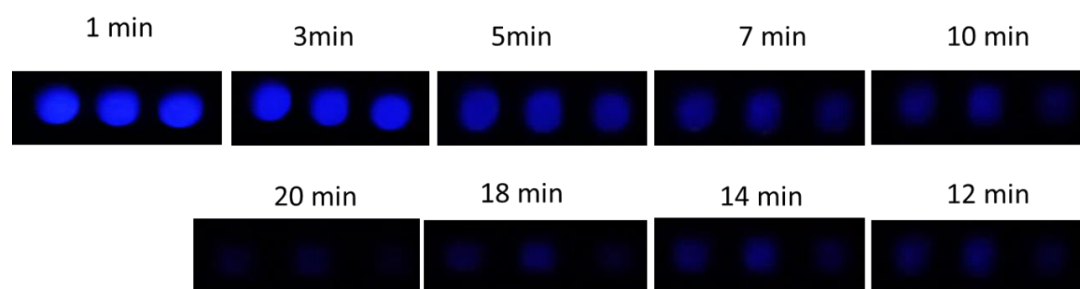

Figure 6.6 eCL imaging signal (stability upto 20 min)

The green line in Figure 6.8a designates the chemiluminescence intensity observed when catalyzed by bare GNPs and its variation as a function of time. The result clearly signifies that bare GNPs have almost no catalytic activity and do not exhibit any eCL. However, when the GNPs are cross-linked with PDT (red line in Figure 6.8a), there is a significant enhancement in the catalytic behavior giving eCL of remarkable intensity. The blue line in Figure 6.8a shows diminished CL intensity, which is due to the addition glucose in reaction system. As per eCL, signal imaging with GNPs-PDT has enhanced and stable for 10 minutes (significant stability for bioimaging) compared to alone GNPs. The eCL imaging signal was verified by eCL spectra, and it was stable for 20 min (Figure 6.6). However, after interaction with glucose, eCL signal imaging showed inhibition. After that, we designed an assay of proof of concept for quantification of glucose in urine sample-based eCL imaging, as shown in Figure 6.8b. The corresponding CL spectra has been shown in Figure 6.7.
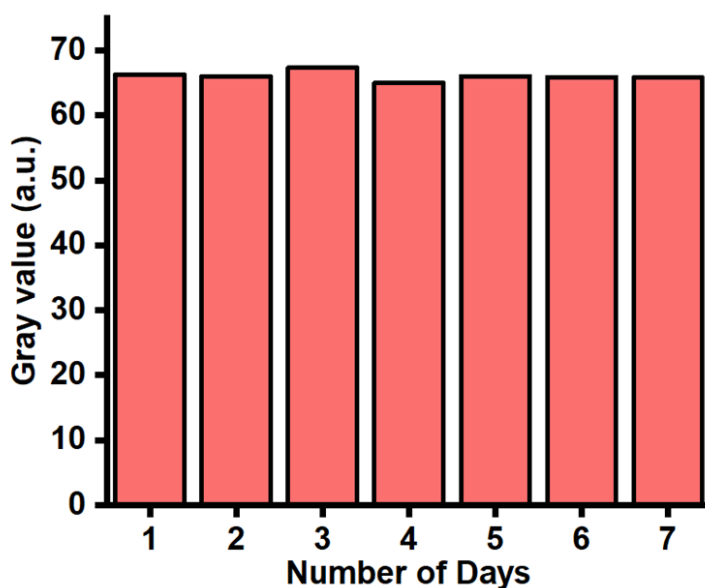
Figure 6.7 Reproducibility study over different days

In this process, the optimized luminol was put in 96 well black plates along with PDT-GNPs and kept in a black box for interaction and chemically produce luminol signal, which was enough to produce an eCL image immediately captured by a smartphone camera and analyzed by Image J for quantification of glucose in urine samples.
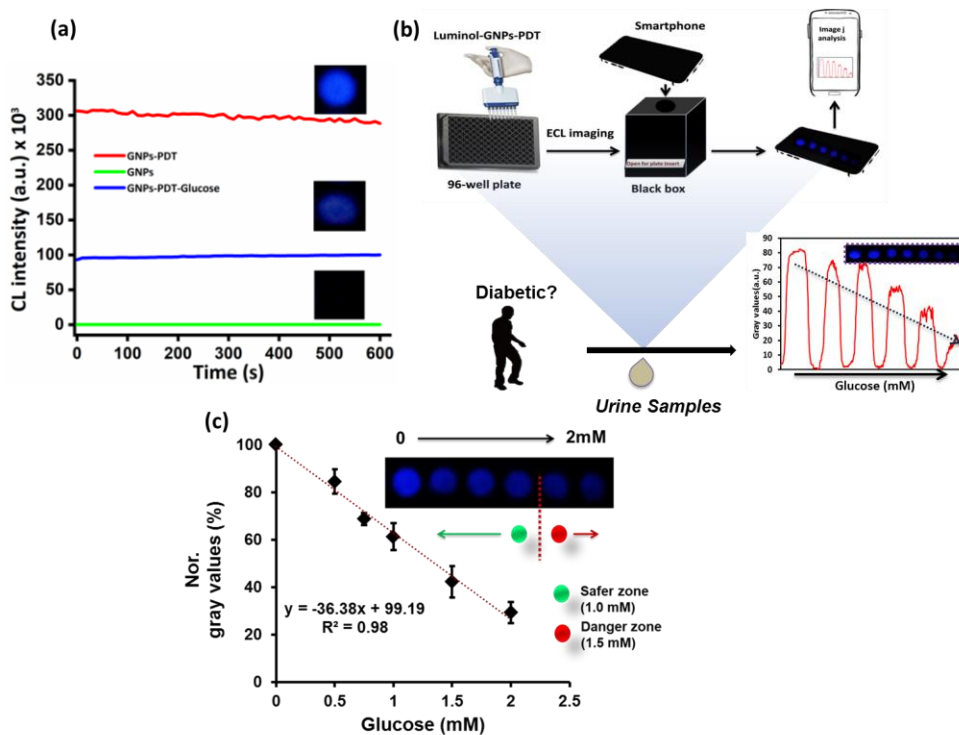

Figure 6.8 Under optimized conditions, (a) validation of eCL imaging stability and enhanced signal, (b) Assay process of proof of concept for quantification of glucose in urine sample using inhibition of eCL imaging signal, and (c) Calibration curve of eCL imaging response in the presence of standard glucose spiked in human urine.

Next, under optimization, we conduct a non-invasive analysis of glucose in urine samples based on luminol-O_2 system imaging. Figure 6.8c depicted glucose sensing based on quenching of eCL imaging with an excellent dynamic range (0.25-2mM), where 1 mM is the normal range of glucose in urine samples; exceeding can cause diabetic problems and the respective

calibration curve is given in Figure 6.8c. At the same time, by means of increasing the concentration of glucose, the eCL imaging response inhibition, demonstrating that the glucose may quench the eCL imaging of the luminol-O_2 system in the presence of catalyst GNPs-PDT [Yang et al., 2021]. As visible in Table 6.1, our non-enzymatic eCL sensor, compared with the other sensors in maximum reported works of sensing approach and bio fluids, exhibited better performance.

Table 6.1 Comparison of non-enzymatic glucose sensors.

Material	Method	Medium	Linear Range (mM)	LOD (mM)	Ref
Cu-MOF	CL	Serum	$0.6 * 10^{-3}$ - $20 * 10^{-3}$	$6 * 10^{-3}$	[Yang et al., 2021]
HRP-AuNPs	Colorimetric	Blood	0.4 to 80	0.4	[Zeng et al., 2012]
AuNPs/O-g-C_3N_4	CL	Sweat	$0 - 200 * 10^{-3}$	$0.1 * 10^{-3}$	[Zhu et al., 2016]
CDs	CL	Blood	0 to 15	$12.6 * 10^{-3}$	[Shen et al., 2020]
CoFe$_2$O$_4$ NPs	CL	Serum	$5.0 * 10^{-5}$ - $1.0 * 10^{-2}$	$1 * 10^{-5}$	[Fan et al., 2012]
ITO/PbS/SiO$_2$ /AuNPs	photo electrochemical	Serum	$1.0 * 10^{-3}$ - 1.0	$0.46 * 10^{-3}$	[Cao et al., 2019]

Att–TiO$_2$	ECL	Serum	1.0 - 1.0 * 10^{-6}	10.0 * 10^{-5}	[Wang et al., 2016]
CS-RGO–NiNPs	Screen-printed electrode	Urine	0.2 - 9	4.1 * 10^{-3}	[Yang et al., 2013]
NiCo$_2$O$_4$	Electrochemical	Urine	1.0 * 10^{-3} -100	0.376 * 10^{-3}	[Chen et al., 2021]
GNPs-PDT	eCL bio imaging	Urine	0.25 -2	0.36	This work

Note: LOD = Limit of detection, CL = Chemiluminescence, ECL = Electrochemiluminescence

6.3.4 Selectivity and interferences

We have done the interference study to know the selectivity of analyte glucose in urine in the ambient of other biological species such as fructose, mannose, lactose, and ions (20 mM concentration) Na$^+$, Cl$^-$, K$^+$, NH$_4$$^{+,}$ and PO$_4$$^{3+}$. The concentrations of glucose and mannose were 2 mM while the concentration of fructose and lactose were 100 μM. Glucose exhibited a significant inhibition effect (Figure 6.9a) that indicates GNPs-PDT possesses good selectivity towards glucose. However, a quenching effect is also shown by fructose, lactose, and mannose. As per the report published by Kawasaki et al., the total fructose excretion in urine by a diabetic patient in a whole day is around 127.8μM, and by a non-diabetic patient is around 37.7μM/day [Kawasaki et al., 2002]. Therefore, fructose is typically present in much lower concentrations in biological samples than glucose, and thus its effect on eCL signals will be less observed in the real sample. Similarly, lactose excretion in the urine is barely detectable. Any lactose not

absorbed by the body is excreted in the feces rather than in urine. However, in some abnormalities and pregnancy lactose may be present but its concentration is nominal to affect our result. Similarly, the concentration of mannose in urine samples ranges from 12-166 μM. In our study, 2000 μM Mannose was taken for interference study, still, it shows less quenching than glucose [Mehta et al., 2018]. Figure 6.9b shows the effect of the interferences like Mannose, Fructose, Lactose, and also its mixtures on glucose sensing, the result clearly signifies the importance of our method giving identical response in the mixture of glucose and every interference with insignificant changes in gray values.
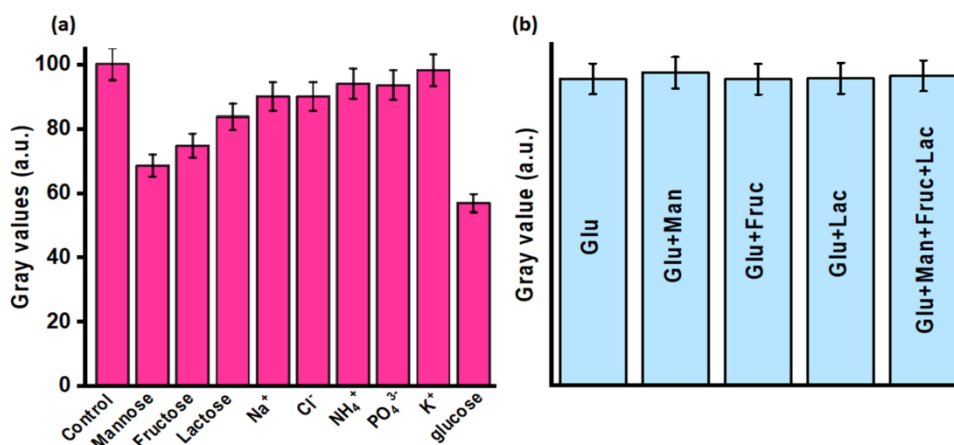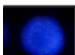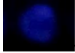

Figure 6.9 Determination of selectivity and interferences in the presence of matching sugar molecules for eCL imaging in urine samples.

6.3.5 Validation of developed sensing system

Analysis of glucose in the real sample (urine) was performed using eCL imaging based on the luminol–O_2 system. Pre-treated urine was centrifuged at 5000 rpm for 30 min to settle down all protein matrices, then applied onto a 96-well black plate. Followed by adding an optimized concentration of reactants, like luminol and GNPs-PDT to perform imaging and

quantify the glucose concentration using Image J analysis. Initially, we spiked different

concentrations of glucose from 0.75 to 2mM, which covered the normal to the diabetic

range, recovery of obtained glucose concentration in urine samples was satisfactory, shown

in table 6.2.

Table 6.2 Glucose spike and recovery in urine samples using eCL imaging

eCL Image	Spike glucose(mM)	Obtained glucose (mM)	Recovery (%)
	0.75	0.7±0.03	94
	1.0	1.1±0.13	110
	2.0	1.9±0.06	95

Finally, we validated the assay by estimating glucose levels in real unknown urine samples.

So, we collected urine samples from 15 volunteers, including healthy and diabetic ones. Figure

6.10 is showing the borderline (1 mM) for glucose concentration, above this level person is

diabetic, and below this is nondiabetic. We applied the obtained gray values of eCL image

analysis on the calibrated platform, and the estimated glucose level was matched with normal

and diabetic patients. The assay was also validated by urine testing in the Biochemistry lab,

IMS BHU by Cobas u 411 urine analyzer. Table 6.3 shows a good correlation between the data

obtained from our proposed method and the urine analyzer supporting the real-time application
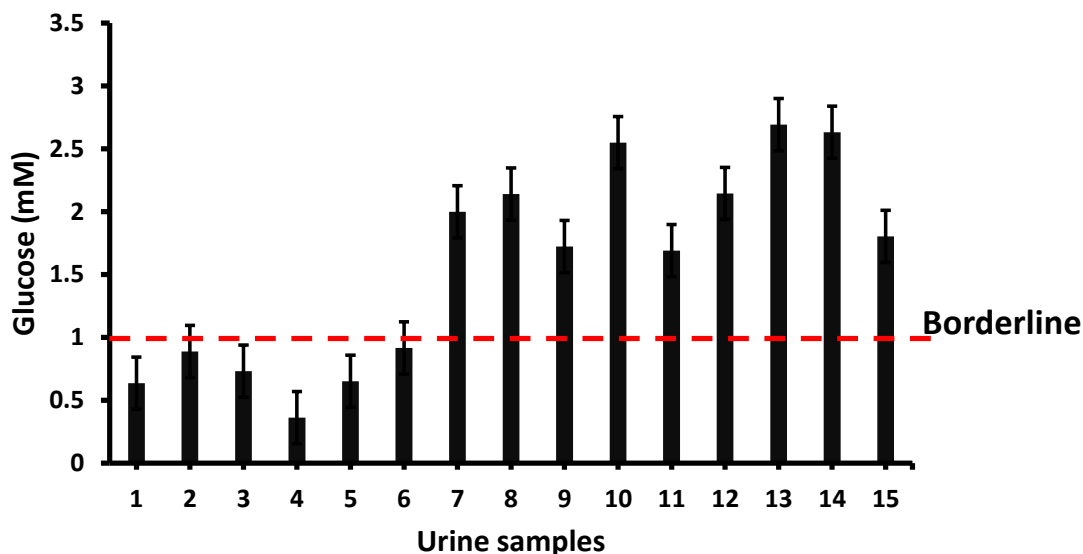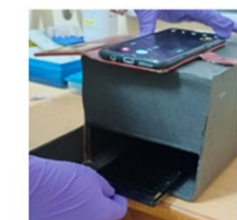
of the developed sensor.

Figure 6.10 Determination of glucose level in 15 volunteers, including healthy and diabetic urine samples (Urine sample obtained from Hospital).

Table 6.3 Comparison of our method with laboratory method for determination of Diabetic conditions

Proposed eCL based glucose detection method using smartphone

Sample No.	Diabetic conditions	
	Our method	Laboratory method
1	Normal	Normal
2	Normal	Normal
3	Normal	Normal
4	Normal	Normal
5	Normal	Normal
6	Normal	Normal
7	Diabetic	Diabetic
8	Diabetic	Diabetic
9	Diabetic	Diabetic
10	Diabetic	Diabetic
11	Diabetic	Diabetic
12	Diabetic	Diabetic
13	Diabetic	Diabetic
14	Diabetic	Diabetic
15	Diabetic	Diabetic

Urine glucose by Cobas u 411 urine analyser

6.4 Conclusions

In this sensing approach, we successfully demonstrated that an easily available smartphone camera is used in imaging and quantification (by Image J) of emitted electromagnetic radiation due to chemiluminescence reactions. Our technique is reliable as well as beneficial over the invasive method (blood sample) for diabetic patients. Hence, we can monitor the glucose level easily without piercing the injection. eCL imaging behavior has been successfully investigated using GNPs-PDT, and glucose was able to suppress the eCL emission light of the luminol-O_2 system. Furthermore, the sensing system revealed good luminol stability and sensitivity, less time-consuming (within minutes), and cost-effective. The developed proof of concept provides a promising way to develop an efficient sensor in biomedical applications to detect cancer biomarkers and other clinically important biomolecules.